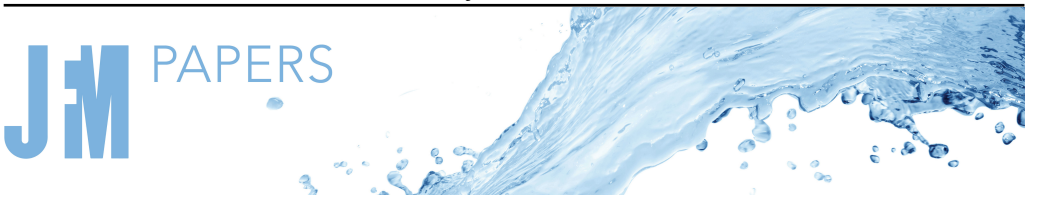
J. Fluid Mech. (2025), *vol.* 1007, A39, doi:10.1017/jfm.2025.73



Modelling pinching dynamics in thin films of binary mixtures

A. Choudhury[1,2], **L. Duchemin**[1], **F. Lequeux**[2] **and L. Talini**[3]

[1]PMMH, CNRS, ESPCI Paris, Université PSL, Sorbonne Université, Université de Paris, 75005 Paris, France.

[2]CNRS, SIMM, ESPCI Paris, PSL Research University, Sorbonne Université, 75005 Paris, France

[3]CNRS, Surface du Verre et Interfaces, Saint-Gobain, 93300 Aubervilliers, France

Corresponding authors: Anjishnu Choudhury, anjishnu.choudhury@espci.fr

(Received 30 May 2024; revised 8 January 2025; accepted 9 January 2025)

In binary mixtures, the lifetimes of surface bubbles can be five orders of magnitude longer than those in pure liquids because of slightly different compositions of the bulk and the surfaces, leading to a thickness-dependent surface tension of thin films. Taking advantage of the resulting simple surface rheology, we derive the equations describing the thickness, flow velocity and surface tension of a single liquid film, using thermodynamics of ideal solutions and thin film mechanics. Numerical resolution shows that, after a first step of tension equilibration, the Laplace-pressure-driven flow is associated with a flow at the interface driven by an induced Marangoni stress. The resulting parabolic flow with mobile interfaces in the film further leads to its pinching, eventually causing its rupture. Our model paves the way for a better understanding of the rupture dynamics of liquid films of binary mixtures.

Key words: foams, thin films, lubrication theory

1. Introduction

The lifetimes of foams and surface bubbles are primarily governed by the drainage and rupture processes of the thin liquid films surrounding bubbles. These processes are influenced by various intricate – and sometimes difficult to control – factors, including contamination Lhuissier & Villermaux (2012), physicochemical properties of added surfactants (Petkova *et al.* 2020), evaporation Pasquet *et al.* (2022), biomolecules (Choudhury *et al.* 2021) and history of thin film formation (Klaseboer *et al.* 2000; Zawala *et al.* 2023), which may induce variations in lifetimes over several orders of magnitude. In the presence of surface-active species, a comprehensive description of the drainage of thin films is made difficult even in controlled conditions, particularly because of

© The Author(s), 2025. Published by Cambridge University Press.

https://doi.org/10.1017/jfm.2025.73 Published online by Cambridge University Press

the coupling of flow with the concentration field of the species. Further complexity arises from the timescales of surface and bulk exchanges of surfactant, which can be comparable to the drainage time (Petkova *et al.* 2021). Generally, the surface rheology that results from those effects is accounted for by using a velocity boundary condition corresponding to an immobile interface with air (Aradian *et al.* 2001), leading to a Poiseuille flow within the film. Although this is a fair assumption for an interface with concentrated surfactants, culminating in a simple lubrication equation for film thickness, it decouples the interfacial shear-stress from the bulk flow caused by drainage. Imposing mobile interfaces, and accounting for the continuity of tangential stress, one can obtain an integro-differential equation for filmheight (Yiantsios & Davis 1990). However, inclusion of additional Marangoni stress necessitates additional evolution equations for closure. This has been done in the past to some extent (Chan *et al.* 2011; Frostad *et al.* 2013) where the parabolic flow is coupled with empirical surface tension variations. Breward & Howell (2002) present a mathematically robust model for a linear variation of surface tension with surfactant concentration, an approximation that is valid only for dilute solutions. The complex surface rheology generally exhibited by surfactant solutions prevents the universality of models.

Recently, the foaming of oil mixtures has attracted renewed interest (Chandran Suja *et al.* 2018; Lombardi *et al.* 2023). The relatively stable foams that can form in these mixtures without any surfactant have been evidenced decades ago (Ross & Nishioka 1975) and are currently observed in many processes of the oil industry, for example, car tank filling and crude oil extraction, or in the food industry, for instance, in frying oils. Anti-foaming molecules are then often required to increase efficiency (Pugh 1996). In the absence of evaporation, it has been shown that the enhanced lifetimes of thin films in mixtures stem from slight differences between the bulk and surface concentrations of different species, leading to thickness-dependent surface tensions of thin films (Tran *et al.* 2020, 2022). Since the diffusion times of small molecules are very short, bulk and interfaces can be considered to be in thermodynamical equilibrium (the time for a molecule to travel across the thickness of a film is $h^2/D \sim 1$ ms for a $1-\mu$m-thick film and taking a typical diffusion coefficient, $D \sim 10^{-9}\mathrm{m}^2\,\mathrm{s}^{-1}$). Thus, the surface rheology of mixtures reduces to Gibb's elasticity (Tempel *et al.* 1965). It leads to an increasing surface tension of a film with decreasing thickness. Since the concentration differences at stake remain very small, the variation of surface tension with concentration is linear. In addition, the disjoining pressure in a film is purely attractive, therefore binary oil mixtures constitute much simpler systems than surfactant solutions to study the drainage mechanisms of liquid films. Existing models developed for the pinching of films of surfactant solutions cannot predict quantitative lifetimes observed in thin films of binary mixtures (Tran *et al.* 2022).

In the presence of Marangoni effects, the process of film drainage and rupture may be divided into three stages (Lhuissier & Villermaux 2012). The first stage comprises the thin film formation; from spherical surfaces to locally flat surfaces. In the case of binary mixtures, this shape is described using a mechanism of equilibration of film tension by a balance between surface tension gradient and the pressure gradient due to Laplace pressure difference. This is reached in a few milliseconds. Naturally, a second stage dynamics ensues, relaxing the pressure gradient and resulting in a more complicated film drainage scenario. The relaxation causes the film to drain via dimpled (marginal) pinching, as also described in soap films (Aradian *et al.* 2001; Trégouët & Cantat 2021). At one point, the film becomes so thin that a third stage of van der Waals attraction becomes effective and causes spontaneous rupture (Shah *et al.* 2021). The film lifetime is mostly determined by the second stage of film drainage when a pinched part reaches a critical thickness, which

https://doi.org/10.1017/jfm.2025.73 Published online by Cambridge University Press

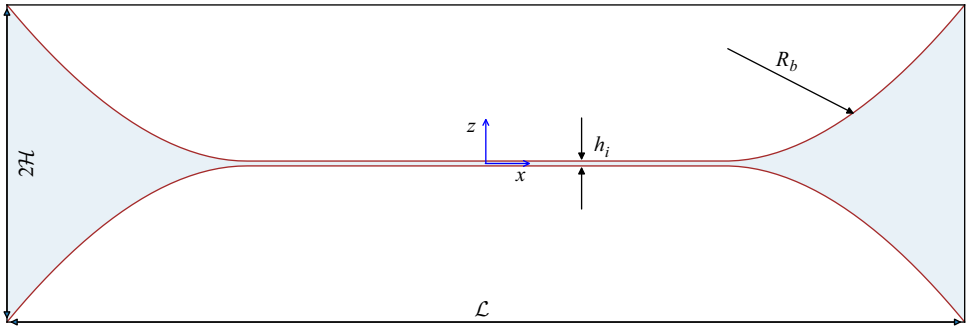


Figure 1. For the scope of this study, we consider a ligament of fluid pinned between two walls at a distance $\mathcal{L}$. Initially, a flat-film profile of thickness, $h_i = 500$ nm, is prescribed in the middle (spanning over $\mathcal{L}/2 = 0.2$ mm) conjoined to a Plateau border of radius, $R_b = 1$ mm, using experimental estimations taken from Tran *et al.* (2022). Using these constraints, we obtain $\mathcal{H} \simeq 16\,\mu$m.

is much longer than the initial viscous stretching phase and the final spontaneous rupture due to van der Waals interactions.

In this article, we model the first two stages of marginal pinching of films of binary mixtures. We follow a similar approach as Breward & Howell (2002) and we do not impose immobile interfaces *a priori*, but instead we consider the coupling of the flow and concentration fields of species. Taking profit of the well-controlled physico-chemistry of mixtures, we obtain an evolution equation for surface tension, here in the context of binary mixtures, using thermodynamic principles of ideal solution theory. As a result, the parameters defining the surface tension gradient are fully determined by the chosen bulk concentration of the mixture species. The pinching dynamics is thus described by three one-dimensional (1-D) coupled evolution equations for film thickness h, mean flow velocity $\overline{u}$ and surface tension γ, which allows a quantitative description of the drainage of thin films and the prediction of their lifetimes.

The article is structured as follows. Section 2 introduces the conservation laws used to model the Marangoni-stress driven system. Section 3 showcases the detailed derivation of the closed-form model using three small parameters in the problem. Further, details of the numerical simulations are described and validated. In § 4, we discuss the main findings of the simulations, specifically focusing on: (i) film tension equilibration and (ii) drainage driven by Marangonistresses generated due to binary mixtures concentration differences. We elucidate our model predictions in comparison with film-thinning laws reported in past experiments/scaling theories, and also contrast with other models in the limiting cases. Finally, we put things into perspective and conclude in § 5.

2. Governing equations

We consider a thin two-dimensional (2-D) liquid film of two miscible liquids, denoted as 1 and 2; the film is bounded by impenetrable walls at $x = \pm\mathcal{L}/2$ and free surfaces at $z = \pm h/2$. Here, $\mathcal{L}$ is the prescribed length of the film and the interfaces are pinned at the walls with a height $2\mathcal{H}$ as shown in figure 1. Since the volume of the film is too small for an equilibrium (parabolic) shape to be reached, the film has to drain and further rupture in the absence of any disjoining pressure. We model the drainage dynamics using conservative laws for mass, momentum and mixture species. In the following, we use subscripts (x, z, t) to denote derivatives $(\partial_x, \partial_z, \partial_t)$ in the equations.

https://doi.org/10.1017/jfm.2025.73 Published online by Cambridge University Press

2.1. *Conservation of mass and momentum*

For mass and momentum balance, we have the Navier–Stokes equations:

$$u_x + v_z = 0, \tag{2.1}$$

$$u_t + uu_x + vu_z = -\frac{P_x}{\rho} + \frac{\mu}{\rho}[u_{xx} + u_{zz}], \tag{2.2}$$

$$v_t + uv_x + vv_z = -\frac{P_z}{\rho} + \frac{\mu}{\rho}[v_{xx} + v_{zz}]. \tag{2.3}$$

Here, ρ and μ are the density and viscosity of the binary mixture which are kept constant; u and v are the velocity components in the x- and z-directions, respectively. Considering the upper interface ($z = h/2$), we have the jump conditions for a free interface. The normal stress balance reads as

$$\boldsymbol{n} \cdot \boldsymbol{T} \cdot \boldsymbol{n} = -\gamma\kappa, \tag{2.4}$$

where $\boldsymbol{T} = -P\boldsymbol{I} + \mu[(\boldsymbol{\nabla u}) + (\boldsymbol{\nabla u})^{\boldsymbol{T}}]$ is the stress tensor, the curvature of the free surface is given by $\kappa = -((h_{xx}/2)/(1 + h_x^2/4)^{3/2})$ and $\boldsymbol{n} = (1/[(1 + h_x^2/4)^{1/2}])([(-h_x/2), 1])$ is the unit normal vector. It is written explicitly as

$$P - \mu\left[\frac{[2v_z(1 - h_x^2/4) - h_x(u_z + v_x)/2]}{1 + h_x^2/4}\right] = \gamma\kappa. \tag{2.5}$$

We also have the tangential stress balance:

$$\boldsymbol{t} \cdot \boldsymbol{T} \cdot \boldsymbol{n} = \nabla_s\gamma, \tag{2.6}$$

where $\mathbf{t} = (1/[(1 + h_x^2/4)^{1/2}])([1, (h_x/2)])$ is the unit tangential vector and $\nabla_s = [\boldsymbol{I\text{-}nn}]\cdot\boldsymbol{\nabla}$ is the curvilinear gradient operator along the interface. It is written explicitly as

$$\mu(u_z + v_x)(1 - h_x^2/4)^{1/2} + \mu h_x(v_z - u_x) = \gamma_x(1 + h_x^2/4)^{1/2}. \tag{2.7}$$

Additionally, we have the kinematic equation for the free surface:

$$h_t + uh_x = 2v. \tag{2.8}$$

Lastly, we take symmetry conditions at $z = 0$:

$$u_z = 0; \quad v = 0. \tag{2.9}$$

2.2. *Conservation of species*

For liquids with typical diffusion coefficient, $D \sim 10^{-9}\,\mathrm{m^2 s^{-1}}$, the equilibrium between the interfaces and the bulk is attained very quickly ($h^2/D \simeq 10^{-5}$s for $h = 100$ nm) as compared with the characteristic time scales of the problem – which range from 10 ms to 10 s. However, the lateral diffusion of species is slow ($L^2/D \simeq 10^3$ s for $L = 1$ mm), so we can fairly neglect it. Consequently, we only take into account lateral advection of species and assume that the system is in thermal equilibrium at a given x-location.

We also introduce the relation between species concentrations of the binary mixture film and its surface tension to couple the flow with the surface tension gradient. Subsequently, we derive an evolution equation for the surface tension based on a volume conservation law for the binary mixture.

Let c_A be the molar fraction of species A (with the lower surface tension) in the bulk and Γ_A be the corresponding molar fraction in the surface layer. Considering a finite thickness of the interface, $\delta \ll h$, the particle numbers per area for species A in a thin differential

https://doi.org/10.1017/jfm.2025.73 Published online by Cambridge University Press

element in x can be written as $w_A = hc_A + 2\delta\Gamma_A$. The flux can be expressed as $j_A = c_A h\overline{u} + \Gamma_A(2\delta)u_s$, where $\overline{u}$ and u_s are mean bulk and interfacial velocities, respectively. Omitting the index A, and using subscripts to denote derivatives, the conservation law for particle numbers per area for species A is written as

$$w_t = -j_x = -(ch\overline{u} + \Gamma(2\delta)u_s)_x. \tag{2.10}$$

We use thermodynamics of ideal mixtures, using a relation known as Butler's equation (Butler 1932; Santos & Reis 2021) to relate the surface molar fraction, Γ_i, to the bulk molar fraction c_i for the species i in an infinite reservoir. Considering the same molar surface σ_i for the two species for simplicity, we have

$$\Gamma_i = c_i e^{(S(\gamma(c_i)-\gamma_i))}, \tag{2.11}$$

where γ_i is the surface tension of pure liquid species i and $S = \sigma_i/RT$ with RT being the molar thermal energy. Therefore, $S(\gamma - \gamma_i)$ is the ratio of the energy cost to replace species i by the mixture at the interface to the thermal energy. For a two species mixture, we have $\Gamma_A + \Gamma_B = 1$ and $c_A + c_B = 1$. This gives the interfacial tension for an infinite reservoir,

$$\gamma(c) = \gamma_B - \frac{\log\left[1 + c(e^{S(\gamma_B-\gamma_A)} - 1)\right]}{S}, \tag{2.12}$$

where c is the free variable for concentration such that $\gamma = \gamma_B$ for $c = 0$ (pure species B) and $\gamma = \gamma_A$ for $c = 1$ (pure species A). Hereafter, we use the index 0 for reference values at infinite film thickness. Equation (2.12) results in a sub-linear variation of surface tension with concentration, as observed in a wide range of binary mixtures. These variations will be later commented on, and shown in figure 2.

3. Reduced order model

In the lubrication limit ($h_x \ll 1$), we expand the flow variables (u, v, P) in a Taylor series with respect to z. The horizontal velocity in the bulk is written as

$$u(x, z) = \overline{u}(x) + u_{Po}(z^2/h^2 - 1/12) + O(z^4), \tag{3.1}$$

where we have intentionally assigned the leading and first-order velocities as $u^{(0)} = \overline{u}$ and $u^{(2)}h^2 = u_{Po}$. This helps us to intuitively realise some quantities described by the species conservation law (2.10). The average velocity $\overline{u}$ is responsible for the shape evolution of the film and the Poiseuille component of the velocity u_{Po} (having by construction a zero mean value) is responsible only for the relative motion of the surface and the bulk, and thus for the non-uniform advection of species. The vertical velocity component v is expanded using continuity (2.1) as

$$v(x, z) = -\overline{u}_x z - (u_{Po})_x\left(z^3/3h^2 - z/12\right) + u_{Po}(2h_x z^3/3h^3) + \mathcal{O}(z^5), \tag{3.2}$$

and the pressure as

$$P(x, z) = P^{(0)} + P^{(2)}\left(z^2 - h^2/12\right) + \mathcal{O}(z^4). \tag{3.3}$$

We put (3.1)–(3.3) into the governing equations for momentum and mass balance (2.1)–(2.9), and find a leading order problem with an unknown surface-tension field $\gamma(x, t)$. Next, using a double expansion Taylor series for the surface tension (for small interfacial thickness and small variation in species concentration), we obtain an evolution equation for $\gamma(x, t)$ using conservation of species (2.10). This provides closure to the leading

https://doi.org/10.1017/jfm.2025.73 Published online by Cambridge University Press

order problem and consequently gives us a set of well-posed evolution equations for $h(x,t)$, $\overline{u}(x,t)$ and $\gamma(x,t)$.

3.1. *Evolution equations for film thickness and averaged velocity*

The following procedure for deriving the thin film hydrodynamics equations is in the spirit of the derivation first done in the seminal work of Eggers & Dupont (1994). Enforcing mass conservation of the film (2.1) into the kinematic equation (2.8) gives us the evolution equation for the film height (Leal 2007), valid at all orders. We thus write the leading order kinematic equation as

$$h_t = -(h\overline{u} + 2\delta u_s)_x \simeq -(h\overline{u})_x, \tag{3.4}$$

Using (3.1)–(3.3) in the x-momentum (2.2), we obtain at leading order,

$$\overline{u}_t + \overline{u}\overline{u}_x = -\frac{P_x^{(0)}}{\rho} + \frac{\mu}{\rho}\left(\overline{u}_{xx} + 2\frac{u_{Po}}{h^2}\right), \tag{3.5}$$

while the z-momentum (2.3) is identically satisfied. Similarly, the interfacial stress conditions given by (2.5) and (2.7) is written at the leading order as

$$P^{(0)} = -\frac{\gamma h_{xx}}{2} - 2\mu\overline{u}_x, \tag{3.6a}$$

$$u_{Po} = \frac{\gamma_x h}{\mu} + \frac{\overline{u}_{xx}h^2}{2} + 2hh_x\overline{u}_x. \tag{3.6b}$$

Note here that the leading order tangential stress condition (3.6*b*) is at $O(z)$. Next, we eliminate $P^{(0)}$ and u_{Po} in (3.5) using (3.6*a*) and (3.6*b*), respectively, and neglect $\gamma_x h_{xx}$ with respect to $\gamma_0 h_{xxx}$ (small surface tension variation) and $2\gamma_x/h$ ($h_x \ll 1$), finally obtaining

$$\overline{u}_t + \overline{u}\overline{u}_x = \frac{1}{\rho h}\left(2\gamma_x + \frac{\gamma_0 h h_{xxx}}{2}\right) + \frac{\mu}{\rho}\frac{(4h\overline{u}_x)_x}{h}. \tag{3.7}$$

Here, γ_0 is the reference surface tension of the liquid mixture at infinite film thickness. We emphasise the subtle point that the 1-D equations (3.4) and (3.7) describes the 2-D velocity field $u(x,z)$. The second-order velocity term u_{Po} enters the leading order problem through (3.6*b*) ensuring tangential stress balance at the interface. As discussed by Tran *et al.* (2022), we have a constant *film tension* at mechanical equilibrium which differs from the interfacial tension. More precisely, in the limit of small curvatures and slopes, the film tension reads $C = \gamma(2 - h_x^2/4 + hh_{xx}/2)$, which is the sum of the interfacial tension at small slopes ($\cos\theta \simeq 1 - h_x^2/8$) and the force due to the Laplace pressure ($\Delta P \simeq \gamma h_{xx}/2$). The first term of the right-hand side of (3.7) can thus be identified as the gradient of film tension C at leading order in h_x. The last term originates from the classical Trouton viscosity which is the ratio of elongational to shear viscosity for planar Newtonian viscous flows appropriate for thin films (Choudhury *et al.* 2020).

We now have the evolution equations for the film thickness $h(x,t)$ (3.4) and the average velocity $\overline{u}(x,t)$ (3.7). To close the system, we need an equation for the unknown surface tension field $\gamma(x,t)$. This is derived in the following subsection.

3.2. *Evolution equation for surface tension of binary mixtures*

To obtain a consistent relation for the surface tension field γ in terms of the species concentration c and film thickness h, we need to define a new variable, the global molar

https://doi.org/10.1017/jfm.2025.73 Published online by Cambridge University Press

fraction (averaged across z),

$$X(x,t) = \frac{w}{h+2\delta} = \frac{ch+2\Gamma\delta}{h+2\delta}. \tag{3.8}$$

In the following, we will use the global molar fraction X as the free variable for species concentration. In fact, if a homogeneous piece of film is stretched at a constant volume, c and Γ both vary because the surface to volume ratio of the film varies, while X remains constant. Thus, the variable X allows us to perform a more comprehensive derivation of the surface tension dependence on species concentration. Subsequently, an explicit relation between X and γ can be deduced using (3.8) and (2.11) in (2.12), giving us the following expression:

$$\gamma(X,h) = \gamma_B - \frac{1}{S}\log\left(\frac{X(2\delta+h)e^{S(\gamma_B-\gamma_A)}}{h+2\delta e^{S(\gamma-\gamma_A)}} - \frac{X(2\delta+h)}{h+2\delta e^{S(\gamma-\gamma_A)}} + 1\right). \tag{3.9}$$

Since the surface tension varies weakly during the whole pinching process (typically differences of $10^{-3}\gamma_0$ are involved in these phenomena Tran *et al.* 2020), we can linearly expand the surface tension of the film. Considering the reference surface tension $\gamma(X_0,\infty) = \gamma_0 = \gamma(c_0)$, with $c_0 = X_0$, we substitute $\gamma_0 = \gamma(c_0)$ for γ on the right-hand side of (3.9) using (2.12). Next, we expand it using Taylor series both in δ and $(X - X_0)$, X_0 being the initial uniform (global) molar fraction. This gives the following exact result at first order in δ and $(X - X_0)$:

$$\gamma(X,h) = \gamma_0 + \frac{\delta}{h}\frac{2(1-X_0)X_0\left(e^{S\Delta\gamma}-1\right)^2}{S\left(1+X_0(e^{S\Delta\gamma}-1)\right)^2} - (X-X_0)\frac{e^{S\Delta\gamma}-1}{S(1+X_0\left(e^{S\Delta\gamma}-1\right))}, \tag{3.10}$$

where $\Delta\gamma = \gamma_B - \gamma_A$. We thus have the linearised version of γ:

$$\gamma(X,h) = \gamma_0\left(1 + \frac{\alpha}{h} - \beta\,(X - X_0)\right). \tag{3.11}$$

The term $\alpha\gamma_0/h$ is the Gibbs elastic modulus of the film, or the variation of the interfacial tension under stretching at constant global molar fraction X (see discussions of Tran *et al.* 2020,2022) whereas β is a positive dimensionless solutal Marangoni coefficient. Both α and β depend on the initial composition of the mixture. Combining (2.11) and (2.12), and using (3.8), we also have

$$\Gamma_0 - c_0 = \frac{(1-X_0)X_0\left(e^{S\Delta\gamma}-1\right)}{1+X_0\left(e^{S\Delta\gamma}-1\right)}, \tag{3.12}$$

which leads to

$$\beta = \frac{1}{\gamma_0 S}\frac{\Gamma_0 - c_0}{X_0(1-X_0)} = \frac{1}{\gamma_0}\frac{\partial\gamma}{\partial c_0} \tag{3.13}$$

and to

$$\alpha = 2\delta(\Gamma_0 - c_0)\beta. \tag{3.14}$$

The expression in parentheses of (3.11) is a dimensionless quantity which is in practice $O(1)$ and is always positive, with the choice $\gamma_A < \gamma_B$. The second and third terms are the thickness-dependent and concentration-dependent corrections, respectively, which are generally at most $O(\delta/h)$. Note that $(\Gamma_0 - c_0)$ and thus α vanish for $X_0 = 0$ and $X_0 = 1$ which corresponds to the case of pure liquids, where there is no Marangoni effect. In the

https://doi.org/10.1017/jfm.2025.73 Published online by Cambridge University Press

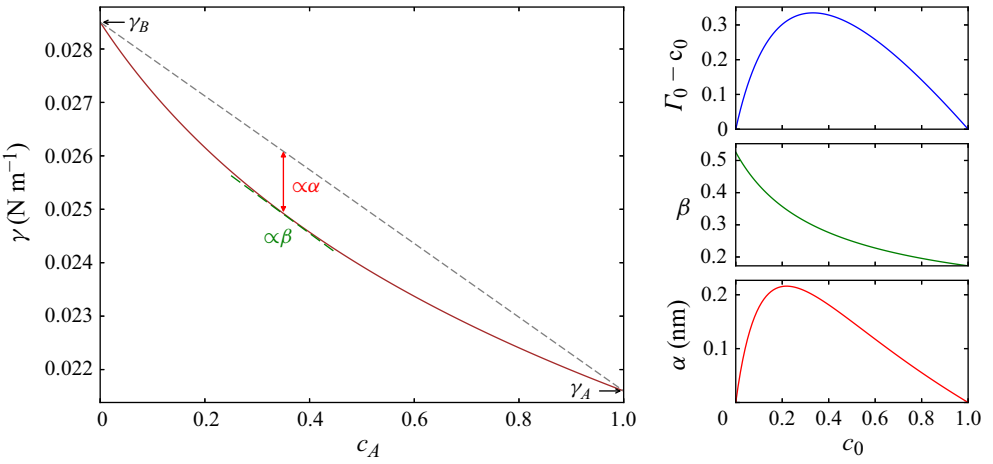


Figure 2. Variation of $\gamma(c_A)$, $(\Gamma_0 - c_0)$, β and α with reference concentration, c_0, for molar surface 2.5×10^5 m^{2}mol^{-1} corresponding to an octane–toluene mixture. The dashed grey line is a straight line for elucidating the sub-linearity of surface tension with mixture concentration.

binary mixtures we consider, containing molecules of similar sizes, the surface tension varies sub-linearly with bulk concentration (Tran *et al.* 2020). This is shown in figure 2 to build intuition. As can be observed in the left panel, α and β characterise this sub-linearity in terms of extent and slope respectively.

Finally, the relation between the global concentration X, the height h and the interfacial tension γ allows us to close the system of equations, leading to the evolution equation for γ. For this, we first evaluate the derivative of (3.11), obtaining

$$\gamma_t = -\alpha\gamma_0 \frac{h_t}{h^2} - \beta\gamma_0 X_t. \tag{3.15}$$

To evaluate X_t, we use (3.8) and easily obtain

$$X_t = \frac{w_t}{h+2\delta} - \frac{wh_t}{(h+2\delta)^2}. \tag{3.16}$$

We now introduce the conservation of species (2.10) and volume, $h_t = -(\bar{u}h + 2u_s\delta)_x$. Note that we have retained the term with surface velocity u_s here, unlike in (3.4). This is done *apriori* to obtain a physically consistent expression for the evolution of global molar fraction X, which must vanish when $(\Gamma - c) = 0$. Using these two laws and after some rearrangement, we obtain the species conservation law written for the global molar fraction X:

$$X_t = -\frac{1}{h+2\delta}(\bar{u}hc_x + u_s 2\delta\Gamma_x) + \frac{(\Gamma - c)}{(h+2\delta)^2}[2\delta\bar{u}h_x + 2\delta(\bar{u} - u_s)_x h]. \tag{3.17}$$

Next, we evaluate the derivative of global molar fraction, X, (3.8) to determine c_x:

$$c_x h = X_x(h+2\delta) + \frac{2\delta(\Gamma - c)h_x}{h+2\delta} - 2\delta\Gamma_x. \tag{3.18}$$

Putting the above expression in (3.17), and in the limit of $\delta \ll h$, we obtain

$$X_t = -\bar{u}X_x + (\Gamma - c)\frac{2\delta}{h}(\bar{u} - u_s)_x + \Gamma_x \frac{2\delta}{h}(\bar{u} - u_s). \tag{3.19}$$

https://doi.org/10.1017/jfm.2025.73 Published online by Cambridge University Press

Here, we realise that the ratio of the third and the second term on the right-hand side is of the order of $\Delta\Gamma/\Gamma \ll 1$. This can be attributed to the indirect relation of Γ with γ due to (2.11) and (2.12). The third term of (3.19) can thus be safely neglected. Evaluating the interfacial velocity as $u_s = u|_{z=h/2}$, we find $(\overline{u} - u_s) = -u_{Po}/6$. If $(\Gamma - c)$ is finite, the parabolic flow contribution will thus advect the bulk and interfacial species differently and the concentration field X will be modified with a flux proportional to $u_{Po}(\Gamma - c)h$. Further, using (3.19) and (3.4) in (3.15), and back-substituting for $X_x = -\gamma_x/\beta\gamma_0 - \alpha h_x/\beta h^2$, we obtain

$$\gamma_t + \overline{u}\gamma_x = \beta\gamma_0\left[\frac{\alpha\overline{u}_x}{\beta h} + \delta\frac{(\Gamma - c)}{3h}(u_{Po})_x\right]. \tag{3.20}$$

The leading order tangential stress condition (3.6*b*) shows that u_{Po} is largely dictated by the surface tension gradient which can be realised by comparing the scales of the terms on the right-hand side. Thus, we substitute $u_{Po} \simeq \gamma_x h/\mu$, retaining only the dominant term. Finally, using (3.14) for α and assuming $(\Gamma - c) \simeq (\Gamma_0 - c_0)$ in (3.20), we obtain the final form of the evolution equation for surface tension:

$$\gamma_t + \overline{u}\gamma_x = \delta\gamma_0\beta(\Gamma_0 - c_0)\left[2\frac{\overline{u}_x}{h} + \frac{1}{3\mu}\frac{(h\gamma_x)_x}{h}\right], \tag{3.21}$$

where the right-hand-side is $O(\delta(\Gamma_0 - c_0)/h)$ and we have neglected higherorder terms. Equations (3.4), (3.7) and (3.21) constitute a closed-form coupled evolution equation necessary to describe the drainage in a thin film of binary mixture. They correspond respectively to the conservation of total mass, momentum and species. The species conservation is indeed contained implicitly in the third equation (3.21) as the surface tension is governed by the species fraction and the thickness.

We can compare our set of equations to those used for the pinching dynamics in the literature. For pure fluids, we have $\Gamma_0 = 0 = c_0$, (3.21) becomes redundant, and thus (3.4) and (3.7) reduces to the system of equations described by Breward & Howell (2002) for pure fluids governed only by viscous stretching (plugflow). Imposing an immobile interface – as done by Aradian *et al.* (2001) – necessitates the use of a different expansion for the parabolic velocity, $u = u^{(0)}(z^2 - h^2/4) + O(z^4)$. Using appropriate interfacial stress conditions, it subsequently gives a single evolution equation for film height: $h_t = -\gamma_0(h_{xxx}h^3)_x/24\mu$, as derived by Aradian *et al.* (2001). This is physically relevant in the limit of concentrated surfactants. However, since tangential stress balance becomes redundant for an immobile interface, Marangoni stresses cannot be included. Lastly, one can also compare our model with the dilute-surfactant model described byBreward & Howell (2002). They model the surface tension evolution using a constitutive law directly relating the surface tension to the surfactant concentration Γ, subsequently deriving a set of evolution equations for h and Γ coupled with an ordinary differential equation for the film tension. That is close to our approach, except the fact that the dynamics of *tension equilibration* cannot be captured in their approach, which is efficiently described in our model due to the evolution equation for velocity (3.7). To the best of our knowledge, our model is the first that captures simultaneously tension equilibration and Poiseuille flow. The *gradient-dynamics* approach (Thiele *et al.* 2016) is another promising direction to build a more comprehensive model and inculcate other complex transport channels like diffusion of species and/or van der Waals forces in a thermodynamically consistent manner. In the next section, we describe the numerical scheme used to solve the three equations of our problem.

https://doi.org/10.1017/jfm.2025.73 Published online by Cambridge University Press

3.3. *Direct numerical simulation*

For the scope of this study, we consider a ligament of fluid pinned between two walls at a distance $\mathcal{L}$ and having a fixed half thickness $\mathcal{H} = \epsilon\mathcal{L}$ at the wall, where ϵ is an aspect ratio. This is close to Scheludko cell experiments, but with an added constraint of confined drainage. However, the pinching dynamics is a localised phenomenon and is expected not to be significantly affected by the far-field conditions. We choose an arbitrary timescale based on capillary emptying defined as $\mathcal{T} = \sqrt{\rho\mathcal{L}^3/\gamma_0}$. The evolution equations (3.4), (3.7) and (3.21) can then be transformed into a simple dimensionless form:

$$H_T = -(\overline{U}H)_\chi, \tag{3.22a}$$

$$\overline{U}_T + \overline{U}\overline{U}_\chi = \left(\frac{H_{\chi\chi\chi}}{2} + 2\frac{G_\chi}{H}\right) + 4\mathrm{Oh}\left(\overline{U}_{\chi\chi} + \frac{H_\chi \overline{U}_\chi}{H}\right), \tag{3.22b}$$

$$G_T + GG_\chi = \frac{M}{3}\left(6\mathrm{Oh}\frac{\overline{U}_\chi}{H} + G_{\chi\chi} + \frac{H_\chi G_\chi}{H}\right). \tag{3.22c}$$

Here, all lengths and time are scaled by $\mathcal{L}$ and $\mathcal{T}$, respectively, using $\chi = x/\mathcal{L}$, $H = h/\mathcal{L}$, $T = t/\mathcal{T}$. Further, the velocity is scaled as $\overline{u} = \overline{U}\mathcal{L}/\mathcal{T}$ and surface tension as $\gamma = G\gamma_0$. We then obtain the following dimensionless numbers: Ohnesorge number, $\mathrm{Oh} = \sqrt{\mu^2/\rho\gamma_0\mathcal{L}}$, and the effective Marangoni parameter, $M = \beta\delta(\Gamma_0 - c_0)\sqrt{\rho\gamma_0/\mu^2\mathcal{L}}$.

The initial conditions for the variables are taken as $G = 1$ and $\overline{U} = 0$. For H, we prescribe a film profile described by a Plateau border of constant radius R_b connected to a flat film at the centre (as also shown in figure 1):

$$H = \frac{h_i/2}{\mathcal{L}} \qquad \text{at } (-\mathcal{L}/4 < \chi < \mathcal{L}/4), \tag{3.23}$$

$$H = \frac{h_i/2}{\mathcal{L}} + \left\{\frac{\chi^2 - (\mathcal{L}/4)^2}{R_b}\right\}/\mathcal{L} \qquad \text{at } (\mathcal{L}/4 < \chi < \mathcal{L}, -\mathcal{L} < \chi < -\mathcal{L}/4). \tag{3.24}$$

Using experimental estimations reported by Tran *et al.* (2022), we prescribe $h_i = 500\,\mathrm{nm}$, $\mathcal{L} = 0.4\,\mathrm{mm}$, $R_b = 1\,\mathrm{mm}$ and $\delta = 1\,\mathrm{nm}$. With these constraints, we obtain an aspect ratio, $\epsilon = 4.1 \times 10^{-2}$. Here, M is set by β, Γ_0, which only depends on the mixture parameters: the concentration c_0, the molar surface σ and the thickness of the interface δ. We have set $\sigma = 2.5 \times 10^5\,\mathrm{m^2\,mol^{-1}}$ for all the simulation data reported. This value is close to those for octane and toluene. For boundary conditions, we have Dirichlet conditions $H = H_0$ and $\overline{U} = 0$ at the two boundaries, whereas a homogeneous Neumann condition is used for G. Note that $G_\chi = 0$ also ensures the additional boundary condition, $H_{\chi\chi\chi} = 0$, required for H through the tension equilibration condition, $HH_{\chi\chi\chi} = 4G_\chi$.

The set of evolution equations (3.22*a*)–(3.22*c*) is solved by using a semi-implicit finite difference scheme on a uniform grid. All the higher derivatives of H, $\overline{U}$ and G are discretised implicitly using central finite difference with second-order accuracy. The timeintegration is done by a first-order accurate Euler forward difference, extrapolated to second-order accuracy using the Richardson extrapolation scheme (Duchemin & Eggers 2014). Further, an adaptive time-stepping scheme is used based on a local error criterion of $E = \max(|H_2 - H_1|)/\epsilon < 10^{-6}$. Here, $H_1 = H(\Delta T)$, $H_2 = H(2 \times \Delta T/2)$. Figure 3 shows a grid convergence study done on the system considered, validating the $O(\Delta\chi^2)$ accuracy of the numerical scheme. Based on it, we prescribe a resolution of $\Delta\chi = 1/600$, which has a relative global error $< 1\,\%$ and a reasonable computational effort. The timestep for the given resolution and error criterion varies within $10^{-3} < \Delta T < 10^{-2}$. The

https://doi.org/10.1017/jfm.2025.73 Published online by Cambridge University Press

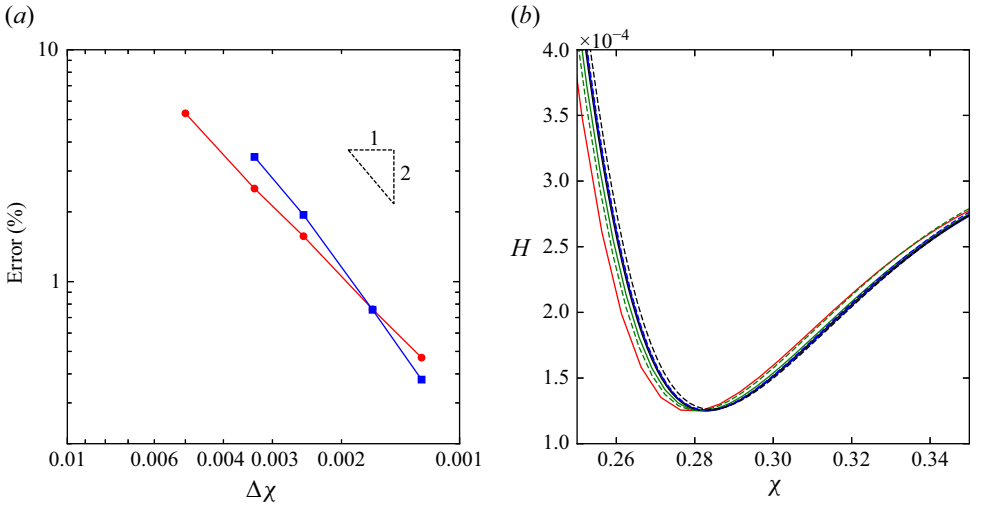


Figure 3. Convergence study of pinching film configuration for $c_0 = 0.02$. (*a*) Relative global error estimation defined by error $= |T - T_{ref}|/T_{ref}$, where T is the time to reach a minimum film thickness of $h = 100$ nm for a given resolution and T_{ref} is the same time for a reference case of $\Delta\chi = 6.25 \times 10^{-4}$. Blue squares are for the $O(\Delta t^2)$ scheme with adaptive time stepping and red squares are for the $O(\Delta t)$ scheme with fixed timestep of $\Delta T = 10^{-3}$. (*b*) Film profiles obtained for different grid resolutions: $\Delta\chi = 0.005$ (red), $\Delta\chi = 0.0025$ (green), $\Delta\chi = 0.0016$ (blue), $\Delta\chi = 0.00125$ (black). Solid lines, $O(\Delta t)$ scheme; dashed lines, $O(\Delta t^2)$ scheme.

code is written in python using the *numpy* library and the discretised semi-implicit linear equations are solved using *linalg.solve* function at a given timestep.

4. Drainage dynamics

We observe that the drainage dynamics clearly splits into two regimes: (i) a fast process of film tension equilibration governed by a plug flow and (ii) a slow process of dimple drainage governed by a Poiseuille flow. Finally, we quantify the effect of Marangoni stress and compare it with models available in the literature for the limiting cases.

4.1. *Film tension equilibration*

The initial tension relaxation process lasts an inertio-capillary time, $\mathcal{T}_c \sim \sqrt{\rho\mathcal{L}^4/\gamma_0\mathcal{H}}$ (Lhuissier & Villermaux 2012). This early dynamics ensures mechanical equilibrium in film tension, C. Figure 4(*a*) shows a typical profile obtained from our model simulation due to an initial stage of tension equilibration. At this moment, the film thickness, h_f, is plotted in figure 4(*b*) for the range of mixture concentrations. It satisfactorily matches the analytical scaling: $h_f \sim \sqrt{\alpha R_f}$, previously derived and experimentally verified by Tran *et al.* (2022), where R_f is the radius at the Plateau border. Moreover, a concentration gradient has formed between the flat film and the meniscus, inducing a Marangoni stress that will further slow down the drainage.

Importantly, the set of equations (3.4), (3.7) and (3.21) is different from the case with an immobile interface assumption. In contrast to the classical approach of prescribing immobile interfaces and excluding plugflow (Aradian *et al.* 2001) to obtain a single-field model for film height, our model describes the leading order plugflow in the film evolution ((3.4), (3.7)) that equilibrates the film tension. However the pressure is not equilibrated and generates a slow Poiseuille flow. This advects differently species at the interfaces and in the bulk, leading to a slow modification of the concentration and thus to the surface tension

https://doi.org/10.1017/jfm.2025.73 Published online by Cambridge University Press

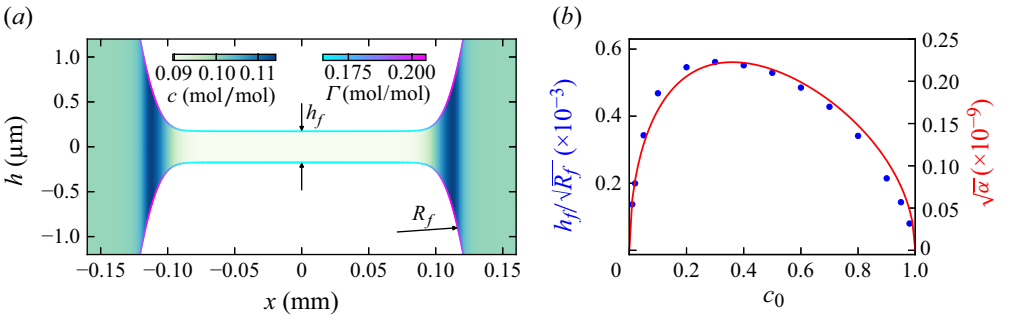


Figure 4. (*a*) Tension equilibrated film profile characterised by film thickness, h_f, and radius, R_f, and corresponding surface (Γ) and bulk (c) molar fraction distribution for a thinfilm of octane–toluene mixture at $t \sim 5 \times 10^{-3}$ s. (*b*) Variation of h_f (blue) and the Gibbs parameter, $\alpha = 2\delta\beta(\Gamma_0 - c_0)$ (red) as a function of the reference bulk molar fraction of octane, $c_0 = [0.01 - 0.98]$.

(3.21). The surface tension evolution in turn modifies the tension equilibrium. Apparently, the parabolic contribution to the viscous stress is of $O(z^2)$ compared with the plug flow that relaxes the tension gradient, and is negligible. However, it is subtly included in the derivation of (3.7) and is the source of non-uniform advection of species and thus of the Marangoni effect, which leads eventually to pinching.

4.2. *Dimpled drainage*

Figures 5(*a*) and 5(*b*) show snapshots for the initial and the final scenarios, respectivly, of the dimple drainage mechanism governed by Poiseuille flow for a typical binary mixture of octane–toluene. The spatio-temporal variations of the flow quantities h, c, Γ are also showcased in the supplementary movie available at https://doi.org/10.1017/jfm.2025.073. Since the surface tension varies inversely with global concentration and with the film thickness, the central part of the film has a higher surface tension. This translates to a Marangoni stress $\sim \partial_x \gamma$ in the negative direction with respect to capillary drainage. Thus, throughout the film evolution, a Marangoni flux opposes the capillary flow, spontaneously maintaining a parabolic flow profile in the bulk, but with a non-zero velocity at the interfaces.

The driving mechanism for film evolution is the surface tension difference via the second term on the right-hand side of (3.21). The overall film evolution dynamics thus work towards minimising this difference (plotted as $\Delta\gamma/\gamma_0$ in figure 5*c*). Since the pressure gradient is concomitant with the surface tension gradient (through the balance of film tension shown in figure 5*f*), it is corollary to say either of the two gradients is minimised during the film evolution. Figure 5(*d*) shows the model predictions of the mean (plugflow) and parabolic (Poiseuille flow) velocities, which asymptotically approach to zero during the remaining process of dimpled drainage. The evolution of curvature at the pinch location, $\kappa = h_{xx}/2$, is shown in figure 5(*e*). In contrast to the earlier study of Aradian *et al.* (2001), we do not observe any scaling with time for the curvature at pinch. More precisely, the curvature at the pinch essentially remains constant throughout the entire duration of pinched drainage. Figure 5(*g*) shows the spatial variation of $\overline{u}$ and u_{Po}. The velocities are clearly less localised than the Laplace pressure gradient. This shows that a change of species concentration induces a velocity in the entire meniscus, predominantly due to tension balance.

https://doi.org/10.1017/jfm.2025.73 Published online by Cambridge University Press

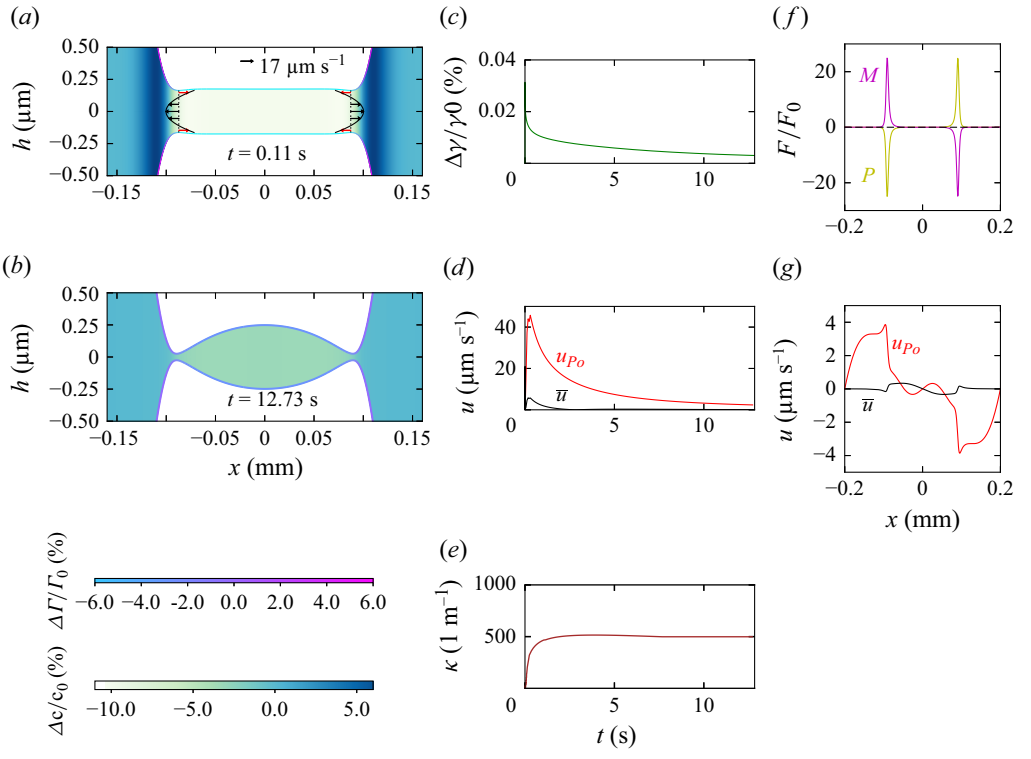


Figure 5. Spatio-temporal evolution of marginal pinching in octane–toluene mixture: (*a*) formation of marginal pinch; (*b*) thickness of the film reaches h_{cut}. The arrows denote the evolved velocity in the film enveloped by the velocity magnitude, at the pinch locations, $\Delta\Gamma = \Gamma - \Gamma_0$ and $\Delta c = c - c_0$, where $\Gamma_0 = 0.1856$ and $c_0 = 0.1$ are reference quantities for surface and bulk molar fraction (for octane), respectively. Evolution of (*c*) $\Delta\gamma = \gamma_{max} - \gamma_{min}$ across the plateau border; (*d*) absolute values of velocities at the pinch location: mean $\overline{u}$ and Poiseuille u_{Po} components; (*e*) maximum curvature, κ, at the pinch location. Across the film length at $t = 12.73$ s: (*f*) dimensionless force/mass due to Laplace pressure gradient $H_{xxx}/2$ (P) and Marangoni stress $2G_x/H$ (M), where $F_0 = 1.73 \times 10^3$ N kg^{-1}; (*g*) mean velocity $\overline{u}$, Poiseuille velocity component u_{Po}.

We now dig deeper into the various mechanisms at play during the film thinning process showcased in figure 6 and in the supplementary movie. Since our initial condition is out of force equilibrium, a plug flow develops causing a *pure stretching* mode which governs the process of equilibration of the film tension, i.e. a surface tension gradient develops which balances the Laplace pressure gradient across the Plateau border. This happens until the inertio-capillary time, $\mathcal{T}_c \sim 10^{-2}$ s. Note that this can be simply realised by observing (3.7), where the source term (in parentheses) is minimised, damped by the Trouton viscosity. The damped oscillations appearing in figure 6 are a manifestation of this process.

From this time onwards, the plug flow is minimised and the process of surface tension gradient relaxation comes into play through (3.21). We thus have a period of transition from a plugflow to a development of a Poiseuilleflow across the thin film.

Once the pressure-driven flow is set up, the main stage of film-thinning follows a power law dependence, $h_{min} \sim t^n$, with a value of $n = -0.66 \pm 0.06$ throughout the range of mixture concentration, c_0. In this context, experimental film-thinning laws for Marangoni-driven systems are scarcely reported, but an exponent of $n = -2/3$ has been experimentally found in the case of thin-film evolution influenced by sparse surfactants (Lhuissier & Villermaux 2012), non-aqueous binary mixtures (Lombardi *et al.* 2023) and

https://doi.org/10.1017/jfm.2025.73 Published online by Cambridge University Press

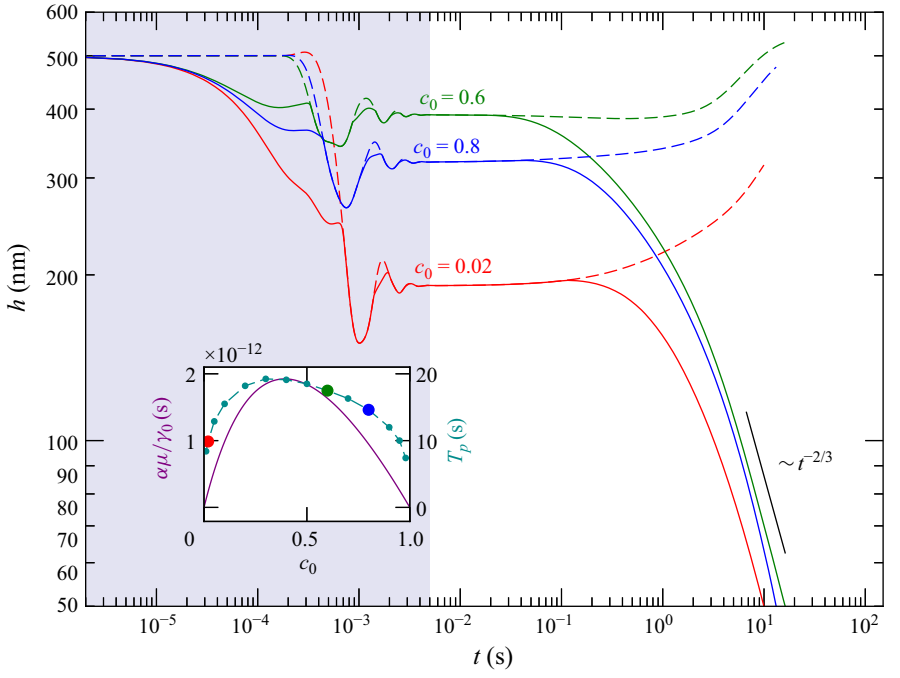


Figure 6. Film evolution at the pinch region, h_{min} (solid curves) and at the centre, h_c (dashed curves) for octane–toluene mixture. The shaded region corresponds to the initial fast process of film tension equilibration. Subsequent relaxation of surface tension leads to the film-thinning law: $h_{min} \sim t^{-2/3}$. The molar surface is $\sigma = 2.5 \times 10^5$ m^2 mol^{-1}. Inset shows model predictions of pinching times of film T_p (teal) compared with $\alpha\mu/\gamma_0$ (purple) for octane–toluene mixture. Colour coded circles correspond to c_0 values of the main plot.

coalescence of emulsion drops (Borkar & Ramachandran 2021). Some scaling theories on analogous systems with mobile interfaces but vanishing Marangoni stress have also reported the same scaling earlier (Yiantsios & Davis 1990; Frostad *et al.* 2013). Our model, where the interfacial velocity is governed by a surfactant-like effect predicts close to this scaling. Earlier models (Klaseboer *et al.* 2000; Aradian *et al.* 2001; Shah *et al.* 2021) for a similar geometry involving Plateau borders, relevant to thin films in foams, predict a scaling exponent of $n = -1/2$ when a Poiseuille flow with immobile interfaces is considered.

Our model predictions of film lifetimes is shown in figure 6 (inset) as a function of mixture concentrations. To estimate the film lifetime, we choose a cutoff film thickness, $h_{cut} \sim 50$ nm, when it is safe to assume that van der Waals force causes spontaneous rupture. A precise discussion of the role of Van der Waals force (Shah *et al.* 2021) shows that it marginally modifies the pinching dynamics and that the assumption of rupture occurring when $h = h_{cut}$ is fair. It has been reported earlier experimentally that the lifetimes of foams and surface bubbles of binary mixture (translated to a lengthscale) correlate with the Gibbs modulus parameter, α (Tran *et al.* 2022). Our model reveals a similar correlation, predicting non-monotonous behaviour with mixture concentration and is thus able to account for experimental observations despite the geometrical differences.

https://doi.org/10.1017/jfm.2025.73 Published online by Cambridge University Press

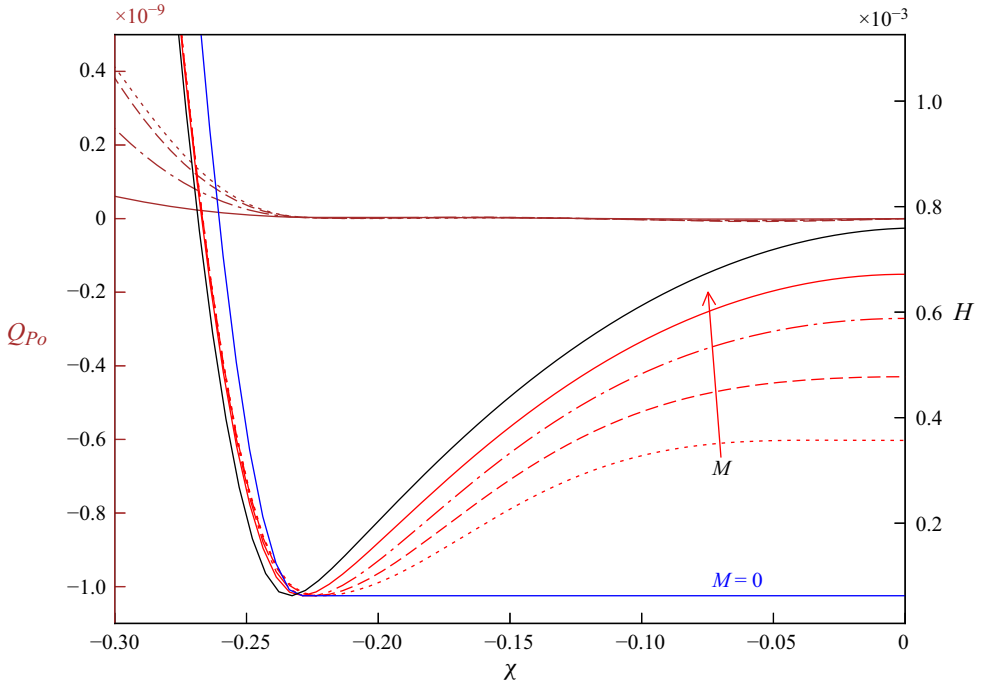


Figure 7. Film profiles (red) and flux due to the parabolic part of velocity profile (brown) at $T = T_p$ for varying Marangoni number, $M = 2.72 \times 10^{-6}$ (dotted), $M = 5.4 \times 10^{-6}$ (dashed), $M = 1 \times 10^{-5}$ (dash-dotted) and $M = 2.48 \times 10^{-5}$ (solid). The blue solid line is for a pure liquid case ($M = 0$), where drainage occurs via viscous stretching (plug flow). The black solid line is the prediction for the model with immobile interface. $\gamma_0 = 2.17 \times 10^{-2}$ N/m for red and blue solid lines. The initial conditions for h is the same as described in figure 1 for all the cases.

4.3. *Effect of Marangoni stress*

We finally present quantitative data on how the flow driven by Marangoni stress manifests. Note that the material parameters determining the Marangoni effect enter the problem through the combined Marangoni parameter M (3.22*c*).

Figure 7 shows film profiles for various values of M. As discussed after (3.19), the parabolic flow contribution advects bulk and interfacial species differently, modifying X with a flux $\propto (\Gamma - c)u_{Po}h$. Since $u_{Po} \sim \gamma_x h/\mu$, we have the flux due to the parabolic part of the velocity profile, $Q_{Po} \sim G_\chi H^2/\mathrm{Oh}$, in dimensionless form, assuming $(\Gamma - c)$ to be a constant. We also plot Q_{Po} corresponding to the film profiles.

Marangoni stress $\propto G_\chi$ developed due to the initial tension equilibration induces the flux Q_{Po}. Interestingly, we observe that a larger Marangoni number results in a weaker Q_{Po} across the pinched region, which can be attributed to larger interfacial velocities competing with the bulk drainage. This leads to slower advection of the species concentration (X) translating to slower relaxation of G_χ and thus longer pinching time, T_p.

It is noteworthy that as $M \to 0$, the dimpled region shrinks to zero and the film becomes flat at the centre corresponding to a pure viscous stretching solution with $t_p \sim 10^{-2}$ s. However, as soon as a finite $M > 0$ is introduced, the dynamics changes completely due to the paradigm shift from a fast plug flow ($h \sim t^{-2}$) to a slow parabolic flow ($h \sim t^{-2/3}$), leading to a dimpled solution with $t_p \sim 10$ s. We have also plotted the prediction for a case of immobile interface (black solid line) for completeness. This model lies in yet another

https://doi.org/10.1017/jfm.2025.73 Published online by Cambridge University Press

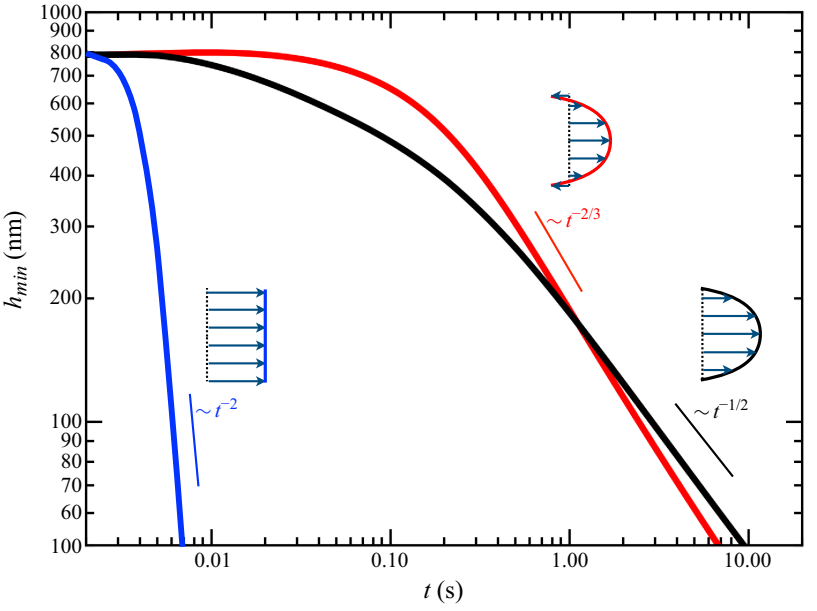


Figure 8. Drainage dynamics of different types of models: black, single-field model for immobile interface (Aradian *et al.* 2001); blue, two-field model for viscous stretching in pure liquids (Breward & Howell 2002); red, three-field model (present work) with $c_0 = 0.1$. We take the same initial film profile (tension equilibrated) with film thickness, $h_i = 800$ nm, and Plateau border radius, $R_b = 2$ mm, for all the models.

different paradigm of pure Poiseuille flow ($h \sim t^{-1/2}$), and thus cannot be recovered as a limiting case of our model with linearised surface tension variations. Our model thus fills the gap between two modelling approaches for Plateau-border-driven thin-film flows. This is showcased in figure 8, where we have plotted predictions of film thinning law for minimum height $h_{min}(t)$ and representative schematic of the velocity profiles across the film thickness, for various class of models. To sum-up, our model that accounts simultaneously for Poiseuille flow and tension equilibrium leads to a scaling for pinching that is different from the classical models that assume either purely Poiseuille flow or only tension equilibrium (viscous stretching).

5. Conclusions

To summarise, we describe the dynamics of marginal pinching in liquid mixtures. Using three small parameters in the problem: $h_x \ll 1$ (lubrication approximation), $\delta/h \ll 1$ (small interfacial thickness) and $(X - X_0) \ll 1$ (small variations in species concentration), we obtain a well-posed set of three coupled evolution equations for film thickness, mean velocity and surface tension. The model accounts for the interplay between capillary drainage and a concomitant Marangoni flow without any presumption on the flow. The parabolic component of the resulting Poiseuille flow is subtly included in the leading order derivation and additionally appears as a second gradient of surface tension. We obtain variations of pinching times for binary mixtures in a canonical geometry of a Scheludko cell that are in agreement with experiments. We observe that the pinching dynamics is a two step process with well-separated time scales, the fast process being governed by tension equilibration with a plug flow and a slower process governed by species advection by Poiseuille flow. Further, the predicted dynamics agrees well with

https://doi.org/10.1017/jfm.2025.73 Published online by Cambridge University Press

qualitative behaviours observed in recent experiments of surface bubbles with sparse-surfactant effects, for example, the *marginal regeneration* reported in contaminated water (Lhuissier & Villermaux 2012), delayed coalescence of droplets of two miscible liquids (Karpitschka & Riegler 2012) and the tension equilibration process reported in salt solutions (Liu *et al.* 2023).

We point out that the estimated pinching times are sensitive to aspect ratio ($\mathcal{H}/\mathcal{L}$), length scales (h_i, R_b, δ) and the Ohnesorge number (Oh), but the estimation of timescale for the marginal pinching process is not trivial and is an interesting objective of a future study. This requires a careful estimation of the dimensions of pinch region, which must correlate to the physicochemical parameters of the binary mixture. We emphasise that the model presented here is versatile in nature, providing a recipe to model other foamy systems governed by negligible delay in adsorption which could be relevant for dilute surfactant-like effects.

Supplementary movie. Supplementary movie is available at https://doi.org/10.1017/jfm.2025.073.

Declaration of interests. The authors report no conflict of interest.

Acknowledgements. The authors thank the anonymous referees whose critical comments and suggestions improved the clarity of the paper. A.C. further thanks Florence Elias, Benoit Scheid and Jaywant Arakeri for intriguing discussions.

References

Aradian, A., Raphael, E. & De Gennes, P.-G. 2001 "Marginal pinching" in soap films. *Europhys. Lett.* **55** (6), 834–840.

Borkar, S. & Ramachandran, A. 2021 Substrate colonization by an emulsion drop prior to spreading. *Nat. Commun.* **12** (1), 5734.

Breward, C. & Howell, P. 2002 The drainage of a foam lamella. *J. Fluid Mech.* **458**, 379–406.

Butler, J. 1932 The thermodynamics of the surfaces of solutions. *Proc. R. Soc. Lond A* **135** (827), 348–375.

Chan, D., Klaseboer, E. & Manica, R. 2011 Film drainage and coalescence between deformable drops and bubbles. *Soft Matter* **7** (6), 2235–2264.

Chandran Suja, V., Kar, A., Cates, W., Remmert, S., Savage, P. & Fuller, G. 2018 Evaporation-induced foam stabilization in lubricating oils. *Proc. Natl Acad. Sci. USA* **115** (31), 7919–7924.

Choudhury, A., Dey, M., Dixit, H.N. & Feng, J.J. 2021 Tear-film breakup: the role of membrane-associated mucin polymers. *Phys. Rev. E* **103** (1), 013108.

Choudhury, A., Paidi, V., Kalpathy, S. & Dixit, H. 2020 Enhanced stability of free viscous films due to surface viscosity. *Phys. Fluids* **32** (8), 082108.

Duchemin, L. & Eggers, J. 2014 The explicit-implicit-null method: removing the numerical instability of pdes. *J. Comput. Phys.* **263**, 37–52.

Eggers, J. & Dupont, T. 1994 Drop formation in a one-dimensional approximation of the Navier–Stokes equation. *J. Fluid Mech.* **262**, 205–221.

Frostad, J., Walter, J. & Leal, L. 2013 A scaling relation for the capillary-pressure driven drainage of thin films. *Phys. Fluids* **25** (5), 052108.

Karpitschka, S. & Riegler, H. 2012 Noncoalescence of sessile drops from different but miscible liquids: hydrodynamic format analysis of the twin drop contour as a self-stabilizing traveling wave. *Phys. Rev. Lett.* **109** (6), 066103.

Klaseboer, E., Chevaillier, J., Gourdon, C. & Masbernat, O. 2000 Film drainage between colliding drops at constant approach velocity: experiments and modeling. *J. Colloid Interface Sci.* **229** (1), 274–285.

Leal, L. 2007 *Advanced Transport Phenomena: Fluid Mechanics and Convective Transport Processes*. Vol. **7**. Cambridge University Press.

Lhuissier, H. & Villermaux, E. 2012 Bursting bubble aerosols. *J. Fluid Mech.* **696**, 5–44.

Liu, B., Manica, R., Liu, Q., Xu, Z., Klaseboer, E. & Yang, Q. 2023 Nanoscale transport during liquid film thinning inhibits bubble coalescing behavior in electrolyte solutions. *Phys. Rev. Lett.* **131** (10), 104003.

Lombardi, L., Roig-Sanchez, S., Bapat, A. & Frostad, J. 2023 Nonaqueous foam stabilization mechanisms in the presence of volatile solvents. *J. Colloid Interface Sci.* **648**, 46–55.

Pasquet, M., Boulogne, F., Sant-Anna, J., Restagno, F. & Rio, E. 2022 The impact of physical-chemistry on film thinning in surface bubbles. *Soft Matter* **18** (24), 4536–4542.

https://doi.org/10.1017/jfm.2025.73 Published online by Cambridge University Press

PETKOVA, B., TCHOLAKOVA, S., CHENKOVA, M., GOLEMANOV, K., DENKOV, N., THORLEY, D. & STOYANOV, S. 2020 Foamability of aqueous solutions: role of surfactant type and concentration. *Adv. Colloid Interface Sci.* **276**, 102084.

PETKOVA, B., TCHOLAKOVA, S. & DENKOV, N. 2021 Foamability of surfactant solutions: interplay between adsorption and hydrodynamic conditions. *Colloids Surf. A: Physico-Chem. Engng Aspects* **626**, 127009.

PUGH, R. 1996 Foaming, foam films, antifoaming and defoaming. *Adv. Colloid Interface Sci.* **64**, 67–142.

ROSS, S. & NISHIOKA, G. 1975 Foaminess of binary and ternary solutions. *J. Phys. Chem* **79** (15), 1561–1565.

SANTOS, M. & REIS, J. 2021 Examination of the butler equation for the surface tension of liquid mixtures. *ACS Omega* **6** (33), 21571–21578.

SHAH, M., KLEIJN, C., KREUTZER, M. & VAN STEIJN, V. 2021 Influence of initial film radius and film thickness on the rupture of foam films. *Phys. Rev. Fluids* **6** (1), 013603.

TEMPEL, M., LUCASSEN, J. & LUCASSEN-REYNDERS, E. 1965 Application of surface thermodynamics to Gibbs Elasticity. *J. Phys. Chem* **69** (6), 1798–1804.

THIELE, U., ARCHER, A. & PISMEN, L. 2016 Gradient dynamics models for liquid films with soluble surfactant. *Phys. Rev. Fluids* **1** (8), 083903.

TRAN, H.-P., ARANGALAGE, M., JØRGENSEN, L., PASSADE-BOUPAT, N., LEQUEUX, F. & TALINI, L. 2020 Understanding frothing of liquid mixtures: a surfactantlike effect at the origin of enhanced liquid film lifetimes. *Phys. Rev. Lett.* **125** (17), 178002.

TRAN, H.-P., PASSADE-BOUPAT, N., LEQUEUX, F. & TALINI, L. 2022 Mechanisms ruling the lifetimes of films of liquid mixtures. *J. Fluid Mech.* **944**, A55.

TRÉGOUËT, C. & CANTAT, I. 2021 Instability of the one-dimensional thickness profile at the edge of a horizontal foam film and its plateau border. *Phys. Rev. Fluids* **6** (11), 114005.

YIANTSIOS, S. & DAVIS, R. 1990 On the buoyancy-driven motion of a drop towards a rigid surface or a deformable interface. *J. Fluid Mech.* **217**, 547–573.

ZAWALA, J., MIGUET, J., RASTOGI, P., ATASI, O., BORKOWSKI, M., SCHEID, B. & FULLER, G. 2023 Coalescence of surface bubbles: the crucial role of motion-induced dynamic adsorption layer. *Adv. Colloid Interface Sci.* **317**, 102916.

https://doi.org/10.1017/jfm.2025.73 Published online by Cambridge University Press